https://doi.org/10.1016/j.nanoen.2021.105862

Eutectic phase behavior induced by a simple additive contributes to efficient organic solar cells

Jiehao Fu[a,b], Haiyan Chen[a], Peihao Huang[a], Qingqing Yu[a], Hua Tang[a], Shanshan Chen[c], Sungwoo Jung[d], Kuan Sun[c], Changduk Yang[d], Shirong Lu [a,*], Zhipeng Kan[a,*], Zeyun Xiao [a,*] and Gang Li [b,*]

[a] *Thin-film Solar Cell Technology Research Center, Chongqing Institute of Green and Intelligent Technology, Chongqing School, University of Chinese Academy of Sciences (UCAS Chongqing), Chinese Academy of Sciences, Chongqing 400714, P. R. China*

[b] *Department of Electronic and Information Engineering, The Hong Kong Polytechnic University, Hung Hum, Kowloon, Hong Kong SAR, P. R. China.*

[c] *Key Laboratory of Low-grade Energy Utilization Technologies and Systems, CQU-NUS Renewable Energy Materials & Devices Joint Laboratory, School of Energy & Power Engineering , Chongqing University, Chongqing 400044, P. R. China*

[d] *Department of Energy Engineering, School of Energy and Chemical Engineering, Perovtronics Research Center, Low Dimensional Carbon Materials Center, Ulsan National Institute of Science and Technology (UNIST), 50 UNIST-gil, Ulju-gun, Ulsan 44919, Republic of Korea*

*Corresponding authors:

E-mail: lushirong@cigit.ac.cn (S.L.); kanzhipeng@cigit.ac.cn (Z.K.);

xiao.z@cigit.ac.cn (Z.X.); gang.w.li@polyu.edu.hk (G.L.)

Abstract

Introducing a small amount of high boiling point solvent additive has been widely regarded as a feasible method to optimize the active layer morphology of organic solar cells (OSCs). However, current additives are initially developed for fullerene based OSCs and the development of additive engineering is lagging behind the development of non-fullerene acceptor based OSCs. Here, a simple and versatile solid additive, 1,4-diiodobenzene (DIB), is introduced to the non-fullerene OSCs. Due to the formation of a eutectic phase between the additive and the non-fullerene acceptor, a desired microstructure with tighter molecular stacking and more ordered molecular arrangement is achieved. As a result, DIB treated OSCs display significantly enhanced performance with a power conversion efficiency (PCE) of 17.72% for ternary device, 17.36% for binary device and 15.03% for thick-film (300 nm) device. Additional advantages of the DIB treatment include excellent device stability, toleration of a wide additive concentration range, and versatility in both polymer and small molecule OSCs. The results highlight the importance of additive engineering in high-performance OSCs and demonstrate the significance of supramolecular interactions.

Keywords: organic solar cells, non-fullerene acceptor, additive, eutectic phase

1. Introduction

Significant advancements in non-fullerene acceptor (NFA) have boosted the field of OSCs[1-8]. The ~18% efficiency, when combined with distinct advantages such as flexible, light weight, tunability, high specific power, radiative hardness[9-11], indicates a bright future of the technology. Most NFA OSCs with high efficiency are achieved under the assistance of solvent additives, such as 1-chloronaphthalene (CN) or 1,8-diiodooctane (DIO)[1, 4, 12-16], with strict volume control which brings an obstacle to device's reproducibility. Furthermore, DIO and CN are initially developed for fullerene-based OSCs in which the phase separation behavior of donor and acceptor are different from their non-fullerene counterparts[17-21]; besides, the low volatility of these two additives may have a negative effect on device's stability owing to the deterioration of the solvent additive residues[22-23]. Therefore, such additives are not necessarily the best choice for the recently-developed high-performance NFA OSCs and it is of great importance to develop new types of additives for NFA OSCs. A few studies have explored substitutes for traditional additives[22, 24-29], however, simultaneously achieving high PCE, stability, and ease of processing remains a challenge in additive engineering.

In this work, we introduce a simple solid additive, 1,4-diiodobenzene (DIB), in NFA OSCs. The PCEs of DIB processed PM6:Y6 based devices are ~17% in a wide DIB concentration range of 10-20 mg/mL (114 wt%- 228 wt% of acceptor). At an optimum DIB concentration of 15 mg/mL, a champion efficiency of 17.36% was obtained, which is one of the highest efficiencies for PM6:Y6-based binary OSCs to

date. We also fabricated devices with thick active layer (300 nm) based on PM6:Y6 system and a PCE of 15.03% was achieved, which is among the highest value for OSCs with over 300 nm active layer to date. More impressively, the DIB-treated devices can maintain over 95% of the initial efficiency after 720 hour's storage in glovebox. Besides the successful application in binary system, 17.72% PCE is achieved in ternary system. And except for polymer OSCs, DIB's versatility is also demonstrated in an all-small-molecule organic solar cell (ASM OSC) based on BTR-Cl: Y6[30], where DIB treatment promotes efficiency from 13.53% to 14.32%. Thermal analysis of the NFA and the additive revealed a eutectic phase[31-32], indicating complex formation between Y6 and DIB which enables tighter molecular stacking and more ordered molecular arrangement as evidenced by morphology studies. The eutectic phase has been observed in binary alloys and supramolecular systems. In this work, it is linked to the photoactive layer morphology and OSC performance improvement.

2. Results and discussion

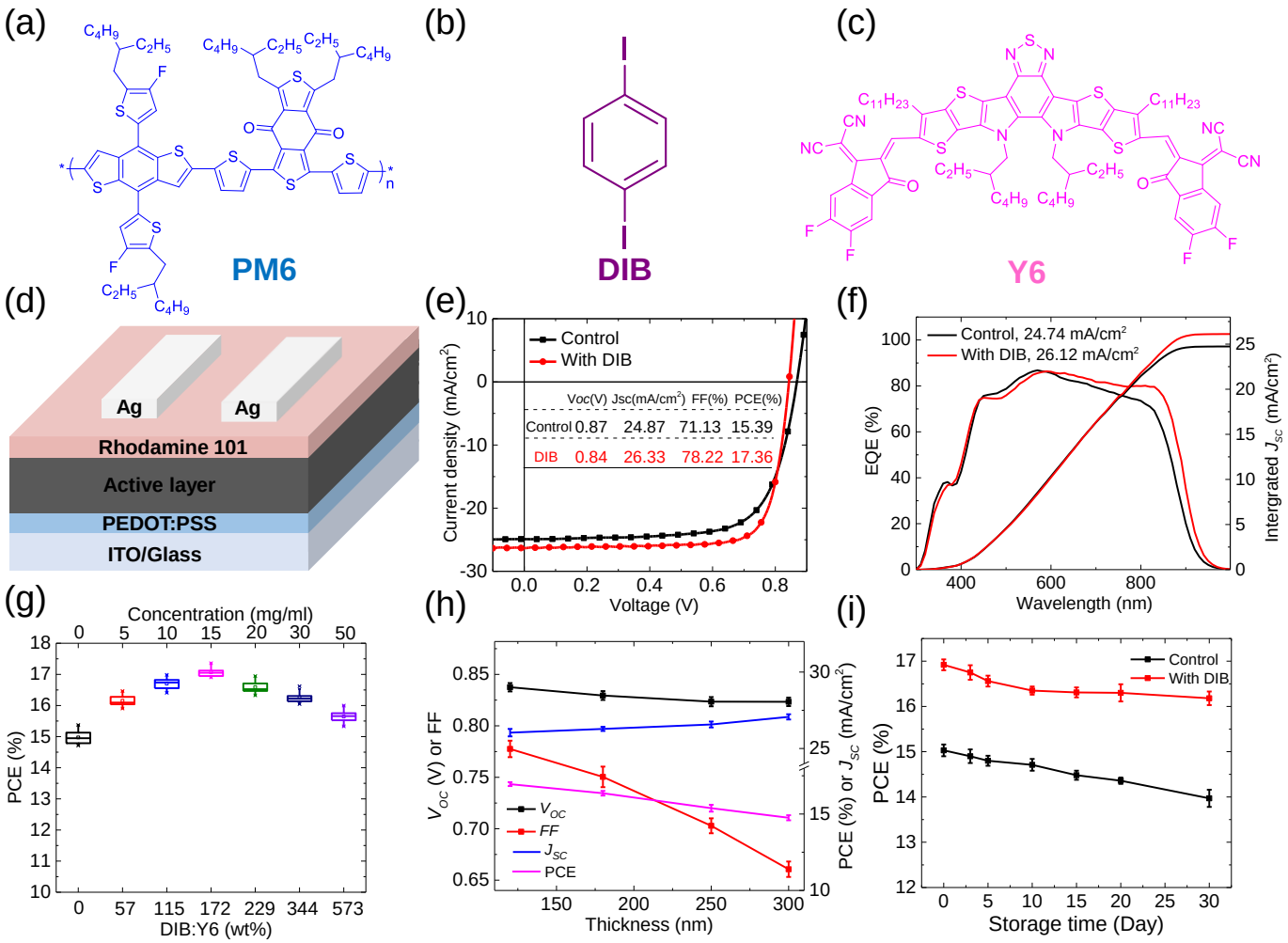

Figure 1. The effect of DIB on the performance of PM6:Y6-based devices. Chemical structures of the polymer donor PM6 (**a**), the solid additive DIB (**b**) and the acceptor Y6 (**c**). (**d**) Schematic illustration of the device structure used in this work. (**e**, **f**) *J*–*V* curves and the corresponding EQE spectra for PM6: Y6-based OSCs with/without DIB. (**g**) PCEs of DIB-treated PM6:Y6 devices as a function of the DIB concentration. (**h**) Performance parameter variations of DIB-treated PM6:Y6 devices under various active layer thicknesses. (**i**) PCE changes of devices with or without DIB as a function of storage time. Note: Devices with DIB were optimized by TA treatment.

As illustrated in **Figure 1**, devices with a normal structure of indiumtin oxide (ITO) / poly (3,4-ethylenedioxythiophene): poly (styrenesulfonate) (PEDOT: PSS)/ PM6:Y6/ Rhodamine 101 inner salt (Rho101) / Ag are fabricated [33]. The detailed

performance parameters of devices with different fabrication conditions are summarized in **Table 1**, the control device shows a highest PCE of 15.39% with an open-circuit voltage (V_{OC}) of 0.87 V, a short circuit current density (J_{SC}) of 24.87 mA/cm^2 and a fill factor (FF) of 71.13%. In contrast, upon introducing DIB additive in precursor solution, the PCE increases to 16.41% at a DIB concentration of 10 mg/mL (**Table S1**). We then conducted a thermal annealing (TA) treatment to remove the residue of DIB in the blend film. After TA at 110 ℃ for 5 min, the DIB (15 mg/mL) treated PCE was further promoted to 17.36% with a V_{OC} of 0.84 V, and a significantly enhanced J_{SC} of 26.33 mA/cm^2 and an excellent FF of 78.22%. To verify the J_{SC} values, we performed external quantum efficiency (EQE) measurements. As shown in **Figure 1f**, the device processed with DIB additive exhibits a higher and broader EQE response in the wavelength range of around 600 nm to 1000 nm compared to the control device, contributing to an improved J_{SC} value of 26.12 mA/cm^2. The integrated J_{SC} values agree well with the value from *J-V* curves. Owing to the excellent volatility of DIB (**Figure S1**), the devices with DIB and TA treatment maintain over 16% efficiency in a wide DIB concentration range of 5-50mg/mL, which promises easier processing for future industrial applications (**Table 1**). We then fabricated PM6:Y6-based OSCs with different thickness. Impressively, DIB-treated devices maintain a good FF of 67.15% even when the thickness of active layer increased to 300 nm (**Figure 1h** and **Table S2**), indicating low charge carrier recombination [34-35]. Owing to the high FF and J_{SC}, over 15% efficiency was realized in thick-film OSCs with an active layer thickness of 300 nm, and set an

efficiency record for binary OSCs with 300 nm thick active layer. Furthermore, we recorded the long-term storage stability of DIB-treated devices in a N_2-filled glovebox. After 720 hour's storage, these devices still maintain an average PCE of 16.18%, over 95% of the initial value (**Figure 1i** and **Table S3**), demonstrating the excellent stability of the DIB processed devices.

Table 1. Detailed photovoltaic performances of PM6:Y6-based devices with different concentration of DIB additive.

Concentration of additive	V_{OC}(V)	J_{SC}(mA cm^{-2})	FF (%)	PCE[c] (%)
0[a] (control)	0.87	24.87	71.13	15.39 (14.97±0.20)
5[b]mg/mL	0.85	25.82	74.63	16.38 (16.15±0.16)
10[b]mg/mL	0.84	26.18	77.28	16.98 (16.70±0.16)
15[b]mg/mL	0.84	26.33	78.22	17.36 (17.06±0.14)
20[b]mg/mL	0.83	26.12	78.17	16.95 (16.59±0.18)
35[b]mg/mL	0.83	26.20	76.42	16.62 (16.25±0.17)
50[b]mg/mL	0.83	25.71	74.96	16.00 (15.64±0.18)

[a]Control devices without any treatment.

[b]Devices performed TA process at 110℃ for 5 min.

[c]The average PCEs with standard deviation calculated from 20 devices.

It is well accepted that the improved J_{SC} and FF are closely related to charge transport, recombination and extraction process[36]. At first, We studied the charge carrier transport properties by using space charge limited current (SCLC) method[37]. **Figure S2** shows the current-voltage ($J^{1/2}$–V) characteristics of the control and DIB-treated samples, the corresponding mobility data are summarized in **Table S5**. For the control device, the mobilities of electron and hole are 3×10^{-4} and 1×10^{-4} cm^2/Vs, respectively. After the treatment of DIB, these two parameters increase to

4×10^{-4} and 3×10^{-4} cm^2/Vs, respectively. The enhanced mobility and more balanced charge transport property are thought to contribute to the increase in J_{SC} and FF.

Because the nanostructures in the photoactive layer have a significant influence on the photovoltaic properties of the devices, we performed tapping-mode atomic force microscopy (AFM) to probe the surface morphology of the blend films. As presented in **Figure 2a** and **2d**, the root-mean-square roughness (Rq) of DIB-treated sample (Rq=1.08 nm) is slightly higher than that of the control one (Rq=0.96 nm), which could be ascribed to the morphology change induced by DIB. Meanwhile, the corresponding phase images (**Figure 2b** and **2e**) obviously reveal that the nanoscale texture of blend varied after DIB processing. Compared with the control sample, DIB-treated film exhibits bigger and more ordered crystals, implying that DIB treatment is an effective method to regulate the phase-separated networks in blend films.

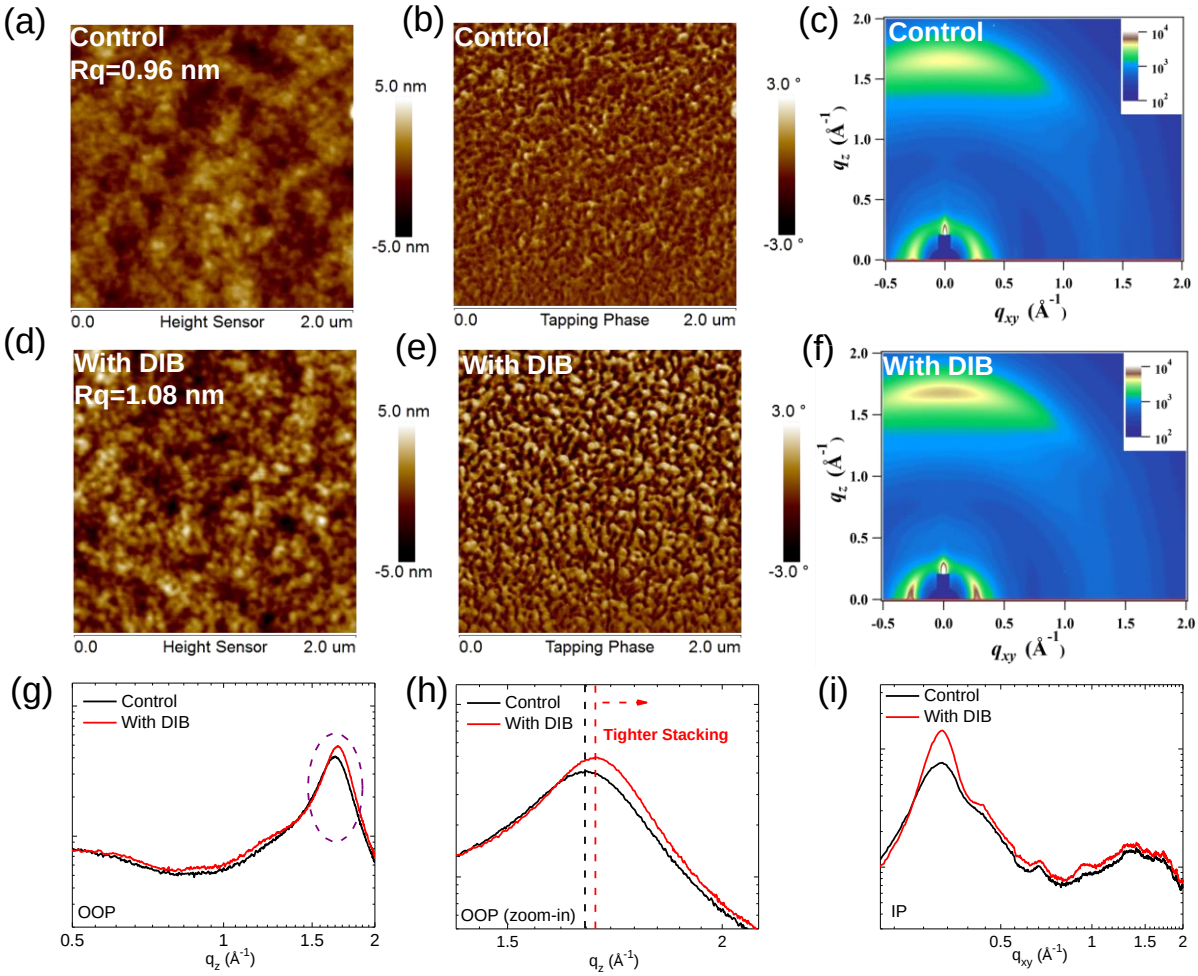

Figure 2. Micro morphology and molecular stacking. AFM height images (**a, d**), phase images (**b, e**) and GIWAXS two-dimensional diffraction patterns (**c, f**) of PM6:Y6 blend films without or with DIB additive. Extracted 1D GIWAXS profiles along the OOP (**g**) and IP (**i**) directions. (**h**) Zoom-in 1D GIWAXS profiles (OOP direction). Note: Blend films with DIB were treated by TA process.

Grazing incidence wide-angle X-ray scattering (GIWAXS) measurement was utilized to further identify the crystalline ordering difference between the control and DIB-modified films. As revealed in **Figure 2c** and **2f**, both two blends show favorable π-face-on orientations in out-of plane direction. **Table S6** summaries the detailed information of (100) and (010) peaks. As we can see, the scattering peak shift (q_z=1.66 Å^{-1} and 1.68 Å^{-1} for the control and DIB-treated sample, respectively) of

(010) diffractions reveals smaller d-spacing and closer π-π stacking in DIB-treated sample, which is beneficial for efficient charge carrier hopping. Meanwhile, according to the Scherrer equation[38], the corresponding π-stacking crystallite coherence length (CCL_{010}) value of the DIB-treated blend (30.25 Å) is larger than the control one (27.60 Å), indicating the relatively larger (010) crystallites contained in the DIB-treated system. Analogously, in in-plane direction, DIB-treated sample exhibits shorter edge-on-(100) distance and significantly larger CCL_{100} value than that of the control sample. The AFM and GIWAXS results jointly demonstrate that DIB processing method assists the self-assembly process, narrows the molecular stacking distances and improves crystalline size. The more condensed and ordered molecular arrangement facilitate the charge transport and extraction processes, and eventually contribute to excellent photovoltaic performance in DIB-treated OSCs.

Futhermore, to understand the thermal behavior and to probe the underlying mechanism, differential scanning calorimetry (DSC) measurement was conducted. At first, we tested the neat DIB, Y6, and their powder-cast mixtures with different weigh ratio, the corresponding results are plotted in **Figure S3** and **Figure 3a**. In the first heating cycle (**Figure S3**), except for the endothermic peak of DIB (T=130 °C), no other endothermic or exothermic behavior can be observed between 50 and 150 °C. However, in the second heating cycle (**Figure 3a**), a new endothermic peak at around 89 °C appears in Y6/DIB mixed sample, indicating the existence of a eutectic phase[31-32], and this endothermic peak becomes more and more significant as Y6 fraction increases. As the phase behavior of powder-cast and solution-cast samples

could be different, we also prepared the solution-cast DIB/Y6 mixtures and found a similar endothermic peak in the first heating cycle (**Figure 3b,** the dash line), demonstrating the fact that eutectic phase behavior exists in an as-cast film from precursor solution with additive. Since there is no endothermic peak for Y6 in both two heating cycles and no new peak in DIB's second heating thermogram, we conclude that this eutectic phase originates from the complex of DIB and Y6.

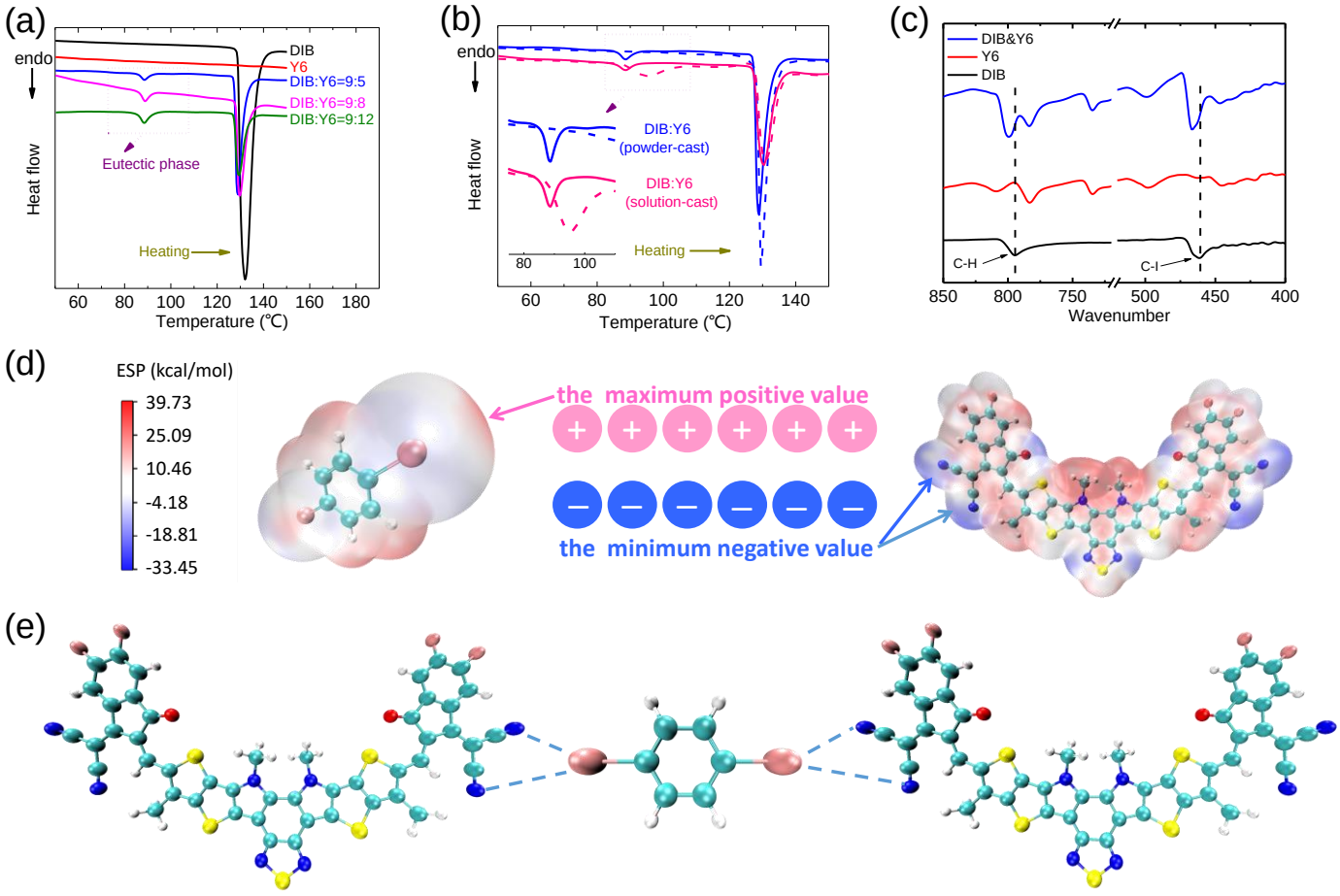

Figure 3. The eutectic phase behavior and it's origin. (**a**) DSC thermograms (the second heating cycle) of DIB, Y6, DIB:Y6 (9:5, w/w), DIB:Y6 (9:8, w/w) and DIB:Y6 (9:12, w/w), these mixtures were prepared by powder-cast method (directly mixing the DIB and Y6 powders in crucible). (**b**) DSC thermograms of DIB:Y6 (9:5, w/w) by powder-cast and solution-cast method (dissolving the mixture of DIB and Y6 in CF and then removing the solvent), the first heating cycles are plotted with dash lines and the second heating cycles are plotted with solid lines. (**c**) FTIR spectra of DIB, Y6, and DIB:Y6. (**d**) The electrostatic potential surfaces of DIB (the left one)

and Y6 (the right one) calculated from the density functional theory (DFT) simulation at the def2-TZVP (DIB) and BLYP/6–31G* level (Y6). (**e**) Proposed interaction mechanisam between DIB and Y6.

To explore the origin of this eutectic phase, we conducted Fourier transform infrared spectroscopy (FTIR) measurements. As presented in **Figure 3c**, the peaks at 795 and 461 cm^{-1} are assigned to the C-H and C-I stretching in neat DIB, respectively. After mixing with Y6, these two peaks shift to 799 and 466 cm^{-1}, respectively. These peak shifts have been reported as signals of halogen-bond interactions between DIB and nucleophiles like nitogen and oxygen atoms[39-40]. In order to get deeper details, we calculated the electrostatic potential surfaces (ESP) of DIB and Y6 by using the DFT simulation (**Figure 3d**). According to computational result, iodine atom in DIB shows the maximum positive value (20.94 kcal/mol), which means this region can form attractive interaction with electron donor sites. And in Y6 molecule, nitrogen atom in cyanogroup shows the minimum negative value (-33.45 kcal/mol), representing the most electron-rich site. So we guess iodine atom in DIB can interact with cyanogroup in Y6, thereby leading to the formation of eutectic phase between DIB and Y6 (**Figure 3e**).

Besides, the effect of this eutectic phase on molecular stacking of Y6 can be demonstrated by the single component film morphology changes induced by DIB additive. As illustrated in **Figure S4**, the neat Y6 film shows a strong π-π stacking peak at $q \approx 1.67$ $Å^{-1}$ ($d = 3.76$ Å) in the OOP direction. Upon addition of DIB, the π-π stacking peak of Y6 shift to $q \approx 1.70$ $Å^{-1}$ ($d = 3.69$ Å), indicating more condensed π-π stacking in Y6+DIB film. AFM studies reveal that Y6 film shows distinct

morphology aggregation after DIB treatments (**Figure S5**) which further confirm the complex formation.

Therefore, we propose that the eutectic phase induced by the halogen bond between iodine atom in DIB and cyanogroup in Y6 should be considered as the intrinsic driving force for denser molecular stacking and more ordered molecular arrangement in the favorable interpenetrating donor/acceptor domains. And, because of suitable volatility (**Figure S1**), the residue of DIB can be removed after thermal annealing process, leaving ideal micromophology and tigher molecular packing.

We also proved the superiority of DIB in PM6:Y6 system, as showed in **Table 2** and **Figure 4a**, DIB contributes to a significant performance improvement, reaching a FF over 78%. Besides, compared to CN and DIO, DIB is much more tolerant to the concentration range (**Figure 4b**), which is benefical to device's reproducibility and industial application.

Table 2. Photovoltaic performance of devices based on PM6:Y6 system with different additives.

Additive	V_{OC} (V)	J_{SC} (mA cm^{-2})	J_{SC}^{cal} (mA cm^{-2})	FF (%)	PCE[a] (%)
CN	0.85	26.07	25.98	71.71	15.97 (15.53±0.29)
DIO	0.82	26.20	25.93	75.72	16.27 (16.01±0.16)
DIB	0.84	26.33	26.12	78.22	17.36 (17.06±0.13)

[cal]The J_{SC} values calculated from EQE tests.

[a]The average PCEs with standard deviation calculated from 20 devices.

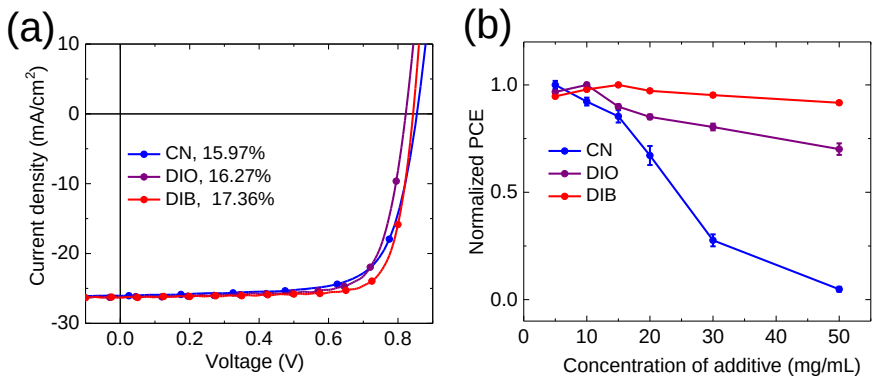

Figure 4. The superiority of DIB. (**a**) J-V curves of PM6:Y6-based devices with different additives. (**b**) PCE changes of devices treated by CN, DIO and DIB as a function of additive concentration range.

To further verify the versatility of DIB as an effective additive, we studied other OSC systems including PBDB-T:Y6, all-small-molecule BTR-Cl:Y6 and PM6:Y6:ICBA based OSCs[30, 41-42]. The relevant molecular structures are presented in **Figure S6**. **Table 3** and **Figure S7** show the effect of DIB on device performance. Obviously, DIB-processing technique is effective in both polymer and small molecule systems, especially enhancing the FF values.

Table 3. Summary of photovoltaic operating parameters for PBDB-T:Y6, BTR-Cl:Y6 and PM6:Y6:ICBA OSCs made with and w/o DIB treatment.

Condition	V_{OC} (V)	J_{SC} (mA cm^{-2})	J_{SC}^{cal} (mA cm^{-2})	FF (%)	PCE[a] (%)
PBDB-T: Y6, Control	0.68	24.33	23.58	57.70	9.55 (9.31±0.13)
With DIB	0.67	25.28	24.73	70.87	12.00 (11.73±0.17)
BTR-Cl: Y6, Control[b]	0.85	23.53	23.27	67.84	13.53 (13.20±0.15)
With DIB[b]	0.84	23.61	23.29	72.22	14.32 (13.92±0.18)
PM6:Y6:ICBA,Control	0.87	25.62	25.39	74.73	16.60 (16.36±0.21)
With DIB	0.84	26.50	26.27	79.62	17.72 (17.40±0.14)

[cal]The J_{SC} values calculated from EQE tests.

[a]The average PCEs with standard deviation calculated from 15 devices.

[b]The electron transport layer (ETL) in BTR-Cl:Y6 device is Phen-NaDPO, as reported in literature[30, 43-44].

3. Conclusion

In summary, we have developed a very simple and effective DIB additive for efficient OSCs. The eutectic phase behavior induced by DIB additive enables tailoring the bulk and surface morphology of the active layer, thereby bringing less charge recombination and more efficient charge transport and extraction processes. Assisted by DIB additive, 17.72%, 17.36%, 15.03% and 14.32% efficiency have been realized in PM6:Y6:ICBA-based, PM6:Y6-based, PM6:Y6-based thick-film (300 nm) and all-small-molecule (BTR-Cl:Y6) binary OSCs, respectively. Furthermore, DIB works effectively in a wide range concentration and the suitable volatility of this additive can help to maintain excellent device stability. The field of OSCs has evolved into a non-fullerene acceptor era with excellent efficiency near commercialization. DIB's success in non-fullerene acceptor system paves an avenue for exploring more effective additive for the industrial application of high-efficiency OSCs.

Appendix A. Supporting information

Supplementary data associated with this article can be found in the online version at doi: ((please add manuscript number))

Acknowledgements

This work was financially supported by research grants from National Natural Science Foundation of China (21801238, 61504015 and 51961165102), the National Youth Thousand Program Project (R52A199Z11), CAS Pioneer Hundred Talents Program B (Y92A010Q10), National Special Funds for Repairing and Purchasing Scientific Institutions (Y72Z090Q10), the Natural Science Foundation of Chongqing (cstc2017jcyjA0752, cstc2018jcyjAX0556, cstc2017jcy-jAX0384, and cstc2018jszx-cyzdX0137), the “artificial intelligence” key project of Chongqing (No. cstc2017rgzn-zdyfX0030), the Key Laboratory of Low-grade Energy Utilization Technologies and Systems (LLEUTS-2017004, LLEUTS-2019001), the Venture & Innovation Support Program for Chongqing Overseas Returnees (cx2017034, cx2019028), and Chongqing Talents Top Youth Talent Program (CQYC201905057), and the Research Grants Council of Hong Kong (C5037-18G).

References

[1] J. Yuan, Y. Zhang, L. Zhou, G. Zhang, H.-L. Yip, T.-K. Lau, X. Lu, C. Zhu, H. Peng, P. A. Johnson, Joule 3 (2019) 1140-1151.
[2] Y. Lin, J. Wang, Z. G. Zhang, H. Bai, Y. Li, D. Zhu, X. Zhan, Adv. Mater. 27 (2015) 1170-1174.
[3] K. Gao, S. B. Jo, X. Shi, L. Nian, M. Zhang, Y. Kan, F. Lin, B. Kan, B. Xu, Q. Rong, Adv. Mater. 31 (2019) 1807842.
[4] K. Jiang, Q. Wei, J. Y. L. Lai, Z. Peng, H. K. Kim, J. Yuan, L. Ye, H. Ade, Y. Zou, H. Yan, Joule 3 (2019) 3020.
[5] Q. Liu, Y. Jiang, K. Jin, J. Qin, J. Xu, W. Li, J. Xiong, J. Liu, Z. Xiao, K. Sun, S. Yang, X. Zhang, L. Ding, Sci. Bull. 65 (2020) 272-275.
[6] Z. Luo, R. Ma, T. Liu, J. Yu, Y. Xiao, R. Sun, G. Xie, J. Yuan, Y. Chen, K. Chen, G. Chai, H. Sun, J. Min, J. Zhang, Y. Zou, C. Yang, X. Lu, F. Gao, H. Yan, Joule 4 (2020) 1236-1247.
[7] J. Huang, H. Tang, C. Yan, G. Li, Cell Rep. Phys. Sci. 2 (2021) 100292..
[8] C. Yan, W. Wang, T.-K. Lau, K. Li, J. Wang, K. Liu, X. Lu, X. Zhan, J. Mater. Chem. A 6 (2018) 16638-16644.

[9] G. Li, Y. Yang, R. Devine, C. Mayberry, Nanotechnology 19 (2008) 424014.
[10] A. Kumar, R. Devine, C. Mayberry, B. Lei, G. Li, Y. Yang, Adv. Funct. Mater. 20 (2010) 2729-2736.
[11] H. Tang, C. Yan, J. Huang, Z. Kan, Z. Xiao, K. Sun, G. Li, S. Lu, Matter 3 (2020) 1403-1432.
[12] Y. Wu, Y. Zheng, H. Yang, C. Sun, Y. Dong, C. Cui, H. Yan, Y. Li, Sci. China Chem. 63 (2019) 265-271.
[13] F. Pan, C. Sun, Y. Li, D. Tang, Y. Zou, X. Li, S. Bai, X. Wei, M. Lv, X. Chen, Energy Environ. Sci. 12 (2019) 3400-3411.
[14] Y. Cui, H. Yao, J. Zhang, T. Zhang, Y. Wang, L. Hong, K. Xian, B. Xu, S. Zhang, J. Peng, Nat. Commun. 10 (2019) 2515.
[15] L. Hong, H. Yao, Z. Wu, Y. Cui, T. Zhang, Y. Xu, R. Yu, Q. Liao, B. Gao, K. Xian, Adv. Mater. 31 (2019) 1903441.
[16] T. Yan, W. Song, J. Huang, R. Peng, L. Huang, Z. Ge, Adv. Mater. 31 (2019) 1902210.
[17] C. Yan, S. Barlow, Z. Wang, H. Yan, A. K.-Y. Jen, S. R. Marder, X. Zhan, Nat. Rev. Mater. 3 (2018) 18003.
[18] P. Cheng, G. Li, X. Zhan, Y. Yang, Nat. Photon. 12 (2018) 131.
[19] Y. He, H.-Y. Chen, J. Hou, Y. Li, J. Am. Chem. Soc. 132 (2010) 1377-1382.
[20] J. C. Hummelen, B. W. Knight, F. LePeq, F. Wudl, J. Yao, C. L. Wilkins, J. Org. Chem. 60 (1995) 532-538.
[21] Y. Liang, Y. Wu, D. Feng, S.-T. Tsai, H.-J. Son, G. Li, L. Yu, J. Am. Chem. Soc. 131 (2009) 56-57.
[22] R. Yu, H. Yao, L. Hong, Y. Qin, J. Zhu, Y. Cui, S. Li, J. Hou, Nat. Commun. 9 (2018) 4645.
[23] B. J. T. D. Villers, K. A. O'Hara, D. P. Ostrowski, P. H. Biddle, S. E. Shaheen, M. L. Chabinyc, D. C. Olson, N. Kopidakis, Chem. Mater. 28 (2016) 876-884.
[24] J. H. Fu, S. S. Chen, K. Yang, S. W. O. Jung, J. Lv, L. K. Lan, H. Y. Chen, D. Q. Hu, Q. G. Yang, T. N. Duan, Z. P. Kan, C. D. Yang, K. Sun, S. R. Lu, Z. Y. Xiao, Y. F. Li, iScience 23 (2020) 100965.
[25] C. Mcdowell, M. Abdelsamie, M. F. Toney, G. C. Bazan, Adv. Mater. 30 (2018) 1707114.
[26] H. J. Jhuo, S. H. Liao, Y. L. Li, P. N. Yeh, S. A. Chen, W. R. Wu, C. J. Su, J. J. Lee, N. L. Yamada, U. S. Jeng, Adv. Funct. Mater. 26 (2016) 3094-3104.
[27] P. Cheng, C. Yan, T. K. Lau, J. Mai, X. Lu, X. Zhan, Adv. Mater. 28 (2016) 5822-5829.
[28] H. Yan, J. Chen, K. Zhou, Y. Tang, X. Meng, X. Xu, W. Ma, Adv. Energy Mater. 8 (2018) 1703672.
[29] L. Liu, Y. Y. Kan, K. Gao, J. X. Wang, M. Zhao, H. Chen, C. J. Zhao, T. Jiu, A. K. Y. Jen, Y. L. Li, Adv. Mater. 32 (2020) 1907604.
[30] H. Chen, D. Hu, Q. Yang, J. Gao, J. Fu, K. Yang, H. He, S. Chen, Z. Kan, T. Duan, Joule 3 (2019) 3034-3047.

[31] C. Muller, T. A. M. Ferenczi, M. Campoy-Quiles, J. M. Frost, D. D. C. Bradley, P. Smith, N. Stingelin-Stutzmann, J. Nelson, Adv. Mater. 20 (2008) 3510-3515.
[32] G. G. Chernik, J. Colloid Interface Sci. 141 (1991) 400-408.
[33] K. Sun, B. Zhao, V. Murugesan, A. Kumar, K. Zeng, J. Subbiah, W. W. Wong, D. J. Jones, J. Ouyang, J. Mater. Chem. 22 (2012) 24155-24165.
[34] N. Gasparini, M. Salvador, T. Heumueller, M. Richter, A. Classen, S. Shrestha, G. J. Matt, S. Holliday, S. Strohm, H. J. Egelhaaf, A. Wadsworth, D. Baran, I. McCulloch, C. J. Brabec, Adv. Energy Mater. 7 (2017) 1701561.
[35] Y. Firdaus, V. M. Le Corre, J. I. Khan, Z. P. Kan, F. Laquai, P. M. Beaujuge, T. D. Anthopoulos, Adv. Sci. 6 (2019) 1802028.
[36] N. A. Ran, J. A. Love, M. C. Heiber, X. Jiao, M. P. Hughes, A. Karki, M. Wang, V. V. Brus, H. Wang, D. Neher, Adv. Energy Mater. 8 (2018) 1701073.
[37] K. Sun, Z. Y. Xiao, S. R. Lu, W. Zajaczkowski, W. Pisula, E. Hanssen, J. M. White, R. M. Williamson, J. Subbiah, J. Y. Ouyang, A. B. Holmes, W. W. H. Wong, D. J. Jones, Nat. Commun. 6 (2015) 6013.
[38] J. Rivnay, S. C. Mannsfeld, C. E. Miller, A. Salleo, M. F. Toney, Chem. Rev. 112 (2012) 5488-5519.
[39] C. Aakeröy, M. Baldrighi, J. Desper, P. Metrangolo, G. Resnati, Chem. - Eur. J. 19 (2013) 16240-16247.
[40] G. Cavallo, P. Metrangolo, R. Milani, T. Pilati, A. Priimagi, G. Resnati, G. Terraneo, Chem. Rev. 116 (2016) 2478-2601.
[41] R. Wang, J. Yuan, R. Wang, G. Han, T. Huang, W. Huang, J. Xue, H. C. Wang, C. Zhang, C. Zhu, Adv. Mater. 31 (2019) 1904215.
[42] Y. J. He, H. Y. Chen, J. H. Hou, Y. F. Li, J. Am. Chem. Soc. 132 (2010) 1377-1382.
[43] D. Hu, Q. Yang, H. Chen, F. Wobben, V. M. Le Corre, R. Singh, T. Liu, R. Ma, H. Tang, L. J. A. Koster, Energy Environ. Sci. 13 (2020) 2134-2141..
[44] H. Tang, H. Chen, C. Yan, J. Huang, P. W. Fong, J. Lv, D. Hu, R. Singh, M. Kumar, Z. Xiao, Adv. Energy Mater. 10 (2020) 2001076.